Intermodal and Subwavelength Energy Trapping in Nonlinear Metamaterial Waveguides

Weijian Jiao and Stefano Gonella

Phys. Rev. Applied **10**, 024006 — Published 7 August 2018

DOI: 10.1103/PhysRevApplied.10.024006

Intermodal and subwavelength energy trapping in nonlinear metamaterial waveguides

Weijian Jiao, Stefano Gonella
Department of Civil, Environmental, and Geo- Engineering
University of Minnesota, Minneapolis, MN 55455, USA

In this work, we experimentally demonstrate the phenomenon of nonlinearity-activated intermodal tunneling in a periodic elastic metamaterial waveguide with internal resonators and we show how this effect can be exploited to achieve conspicuous energy localization and trapping. The architecture of the waveguide is deliberately designed to promote tunneling from flexurally-dominated to axially-dominated modes, in order to accentuate the functional complementarity that can be harnessed during tunneling. 3D laser vibrometry at different scales of spatial refinement is employed to capture global and local in-plane features of the wavefield. The measured response naturally yields an experimental reconstruction of the band diagram of the waveguide and reveals unequivocally the spectral signature of the high-frequency modes that are activated by tunneling. Finally a detailed scan of selected cells highlights a strong and persistent axial activation of the resonators which displays subwavelength deformation features that are unattainable, for the axial mode, by exciting at the same frequency in a linear regime. This result demonstrates the viability of tuning strategies based on nonlinearity and paves the way for the design of metastructures with enhanced energy-trapping and harvesting capabilities.

I. INTRODUCTION

In recent years, acoustic and elastic metamaterials have been the object of considerable scientific interest due to their unique spectral and spatial wave manipulation capabilities. A special feature of the dynamic response of metamaterials is the availability of locally-resonant bandgaps with subwavelength characteristics [1, 2]. The subwavelength attribute results in the possibility to achieve mechanical filtering at relatively low frequencies, or to inject directivity in the long-wavelength limit of the acoustic modes [3]. Recent efforts have been directed towards designing metamaterials endowed with the ability to tune their response to external inputs. Most strategies for tunable and adaptive metamaterials resort to electro-, magneto- or thermo-mechanical effects to modulate their effective mechanical properties [4–7], or to induce microstructural shape changes [8, 9], both effects resulting in a modification of the global phononic characteristics. Other popular tuning strategies for phononic materials rely on instabilities triggered by external loads to induce desired lattice reconfigurations [10–12].

Additional opportunities for wave manipulation are available working with nonlinear metamaterials, such as granular phononic crystals and soft lattice materials [13–15]. Within the discourse on tunability, certain strategies exploit directly the nonlinearity of the medium to actively modify (or enrich) the metamaterial response. For example, the amplitude-dependence of the nonlinear response can be exploited to obtain tunable bandgaps [16–18]. A recent body of work [19–21] has introduced the idea of using nonlinearly-generated higher harmonics and their hopping across modes as a way to enrich the response by tunneling packets of energy from an excited low-frequency mode to a receiving (possibly optical) mode. This phenomenon can result in the activation of high-frequency response features even while operating at relatively low frequencies of excitation. Depending on the dispersive characteristics of the medium and the excitation conditions, we may have two different scenarios of second harmonic generation (SHG). The first one can be referred to as intra-modal hopping: in this case the fundamental and the second harmonic feature compatible modal characteristics, characterized by a high degree of overlap between their respective mode shapes [22–24]. An example is a longitudinal second harmonic generated by a fundamental longitudinal wave in a nonlinear bar. The second scenario is intermodal hopping: here the fundamental harmonic and the second harmonic have orthogonal (or complementary) modal characteristics [19, 25, 26]; an example is a second harmonic involving mostly transversal degrees of freedom generated by a fundamental longitudinal wave in a 3D nonlinear solid. From the perspective of modal enrichment, we are especially interested in cases featuring highly complementary harmonics. As a benchmark example of such scenario, in our previous work [21] we have investigated intermodal hopping between axial and flexural modes in periodic waveguides, with emphasis on the conditions for which phase-matching (resonant) conditions are established between the harmonics. Under these conditions, we have proven that, through SHG, it is possible to transfer packets of energy from a long-wavelength flexural mode, involving predominantly the primary lattice waveguide, to a short-wavelength highly dispersive axial mode that localizes energy in the resonating microstructure. This results in the activation of high-frequency internal cell mechanisms that, in the linear regime, are germane to high-frequency excitations: in other words, if we were operating in the linear regime, an equal activation

of these mechanisms would necessarily require exciting the structure directly at 2ω.

The results mentioned above have so far been confined to the theoretical realm with sporadic experimental verification [15, 27–31]. The objective of this work is to provide a definitive experimental demonstration of the tunneling effects achievable through SHG in elastic metastructures. Our contribution is two-fold. Firstly, while some preliminary evidence of mode hopping in metallic lattices was already given in [31], we here target a significantly stronger signature of energy tunneling by deliberately working with a softer material with more pronounced geometrically nonlinear response. Secondly, by working with a lattice architecture that features a microstructure of resonators, we realize a special class of tunneling mechanisms that can trigger and maximize strong subwavelength energy localization and trapping in the microstructure.

II. EXPERIMENTAL SETUP AND PRELIMINARY ANALYSIS OF LINEAR RESPONSE

The waveguide specimen is manufactured via water-jet cutting from a sheet of acrylonitrile butadiene styrene (ABS) with the following material parameters: Young's modulus $E = 2.1374\,\text{GPa}$, Poisson's ratio $\nu = 0.35$, density $\rho = 1040\,\text{kg/m}^3$. Preliminary experiments carried out on homogeneous strips of the same material suggested that the material has relatively low damping whose manifestation is limited to amplitude attenuation during propagation without any appreciable spectral distortion. For this reason, the viscoelastic effects can be safely ignored in the model used in support of our experiments. The waveguide has dimensions $102\,\text{cm}\times 2\,\text{cm}\times 0.3556\,\text{cm}$ and consists of 56 $1.75\,\text{cm}\times 2\,\text{cm}$ unit cells with internal resonators, as shown in Fig. 1. In order to lower the frequency spectrum of the resonators, we increase their mass by cutting a cylinder core (with radius 0.25 cm) out of the square domain at the center of each unit cell, and inserting a steel disk.

Before we proceed to assess the waveguide's nonlinear response, it is useful to determine its linear dispersive characteristics. For a weakly nonlinear system, the homogeneous component of the nonlinear response has been shown to conform to the dispersion relation of the corresponding linear system [20]. As a result, we can use the linear band diagram to predict certain features of the nonlinear response and to design basic manipulation strategies involving harmonic generation. Specifically, from the inspection of the dispersion branches, we can predict the availability of tunneling mechanisms between the modes, i.e., the existence of $\omega - k(\omega)$ points on a dispersion branch (where ω is the frequency of the excitation and k is the wavenumber) such that the corresponding $2\omega - k(2\omega)$ points fall on a different branch, or on a higher-frequency zone of the same branch. We distinguish between intra-modal (axial-to-axial or flexural-to-flexural) and intermodal (flexural-to-axial) tunneling mechanisms. Our focus here is on intermodal tunneling. We can also identify opportunities for the establishment of phase-matching conditions between fundamental and second harmonic, i.e., when $k(2\omega) = 2k(\omega)$.

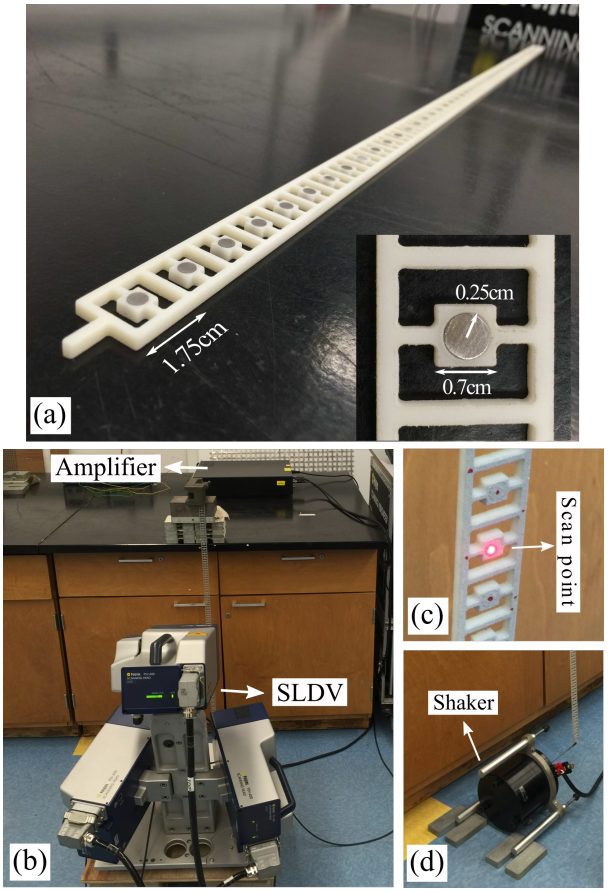

FIG. 1. (a) Waveguide specimen with detail of a unit cell with steel-core resonator. (b) Experiment setup. (c) Detail of the scanned surface. (d) Shaker position for flexural excitation.

We construct a finite element (FE) model of the unit cell using two-dimensional four-node isoparametric elements under plane-stress conditions and we perform a 1D Bloch analysis. In Fig. 2, we plot the band diagram along with the mode shapes at three representative spectral points (one on the flexural branch, two on the axial one). As expected, the two axial mode shapes feature purely axial (axis-symmetric) deformation profiles. Of the two, the one located on the folding part of the branch involves dramatic motion of the resonator. Let us now go through the following three conceptual steps. 1) Let us assume to prescribe a pure-bending excitation at a frequency lying within the range of the flexural mode. We expect the waveguide to experience a deformation that is purely flexural. 2) Let us choose the excitation frequency

such that the nonlinearly-generated second harmonic can hop from the flexural mode to the folding part of the axial mode (close to the frequency cut-off of the mode). Some of the flexural energy externally pumped in the system will be necessarily transferred to cell deformation mechanisms that involve large degrees of axial motion of the resonators relative to the cells. 3) Finally, let us select the frequency-wavenumber excitation pair such that phase-matching conditions are established between the fundamental and the second harmonic. As a result, the magnitude of the observed energy tunneling (and associated trapping events) will be enhanced. This is the sequence of logically concatenated events that we intend to establish, observe and measure in our experiment.

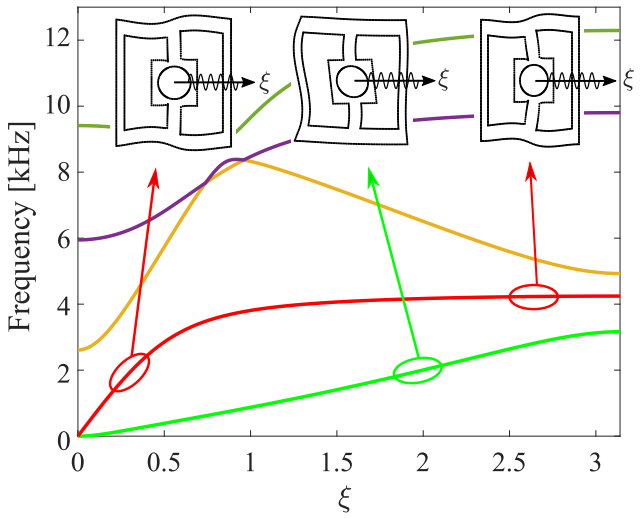

FIG. 2. Band diagram of the waveguide with mode shapes shown for three representative spectral points. ξ is the non-dimensional wavenumber ($\xi = ka$, where k is the wavenumber and a is the length of the unit cell).

Details of the experimental setup are shown in Fig. 1. A 3D Scanning Laser Doppler Vibrometer (SLDV, Polytec PSV-400-3D) is used to measure the in-plane response. The waveguide is hung vertically and clamped at the top end, as shown in Fig. 1(b). The excitation is imparted at the bottom end of the waveguide through an electrodynamic shaker (Bruel & Kjaer Type 4809) powered by a Bruel & Kjaer Type 2718 amplifier. When we intend to excite flexural waves at the fundamental harmonic, the shaker stinger is kept perpendicular to the waveguide and acts on an axial protrusion (visible in Fig. 1a) to engage directly the neutral axis and mimic pure-bending conditions. To excite axial modes, the shaker is rotated to load the tip protrusion axially. It is worth pointing out that, despite a very careful setup, a certian amount of coupling between flexural and axial modes, as well as between in-plane and out-of-plane modes, is inevitable in practice due to unavoidable eccentricities in the stinger and warping of the soft waveguide.

As a next task, we reconstruct the band diagram from the experimental data. We excite the waveguide with a linear chirp with frequency range from 100 Hz to 8 kHz. The in-plane velocity time histories are measured along a straight line of scan points located directly on the resonators (Fig. 1c). These values are aggregated into a matrix of spatio-temporal data and fed to a 2D Discrete Fourier Transform (2D-DFT) to obtain spectral amplitude maps. In Fig. 3a and Fig. 3b, we plot the spectral amplitude of the lateral and axial components of the response obtained through excitations prescribed laterally and axially, respectively. To better resolve the steering region of the axial mode, the chirp is locally replaced by a tone-burst with carrier frequency falling inside the desired interval (Fig. 3c). The dispersion relations obtained from the FE model are superimposed as dashed lines for comparison. Visual inspection suggests a very good agreement between experiments and model (we note a discrepancy of the cut-off frequency prediction for the axial mode, most likely due to an insufficiency of the finest FE mesh that we could afford in our desktop model).

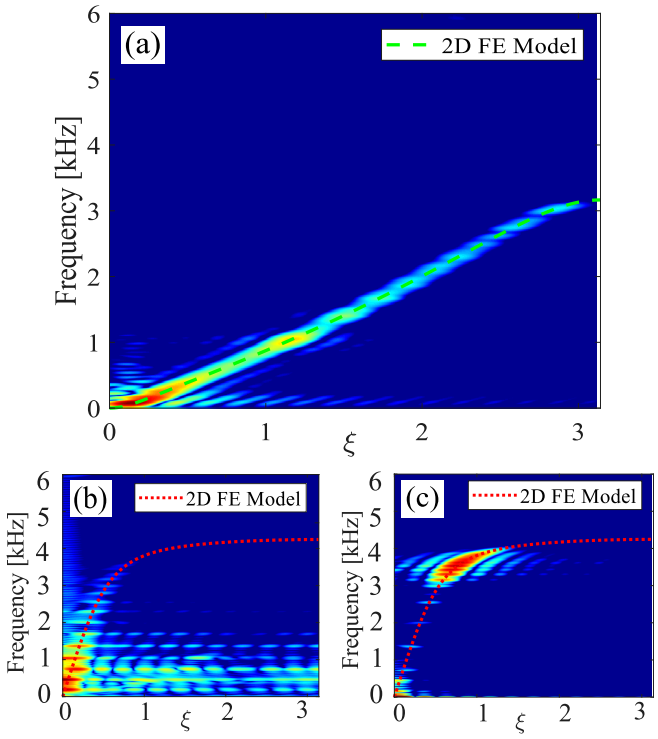

FIG. 3. Experimentally reconstructed spectral response and comparison to FE data. (a) Lateral velocity field. (b) Non-dispersive region and (c) steering region of the axial mode.

III. EXPERIMENTAL EVIDENCE OF INTERMODAL TUNNELING

We can now rely on the band diagram of Fig. 2 to find the excitation conditions necessary to trigger inter-

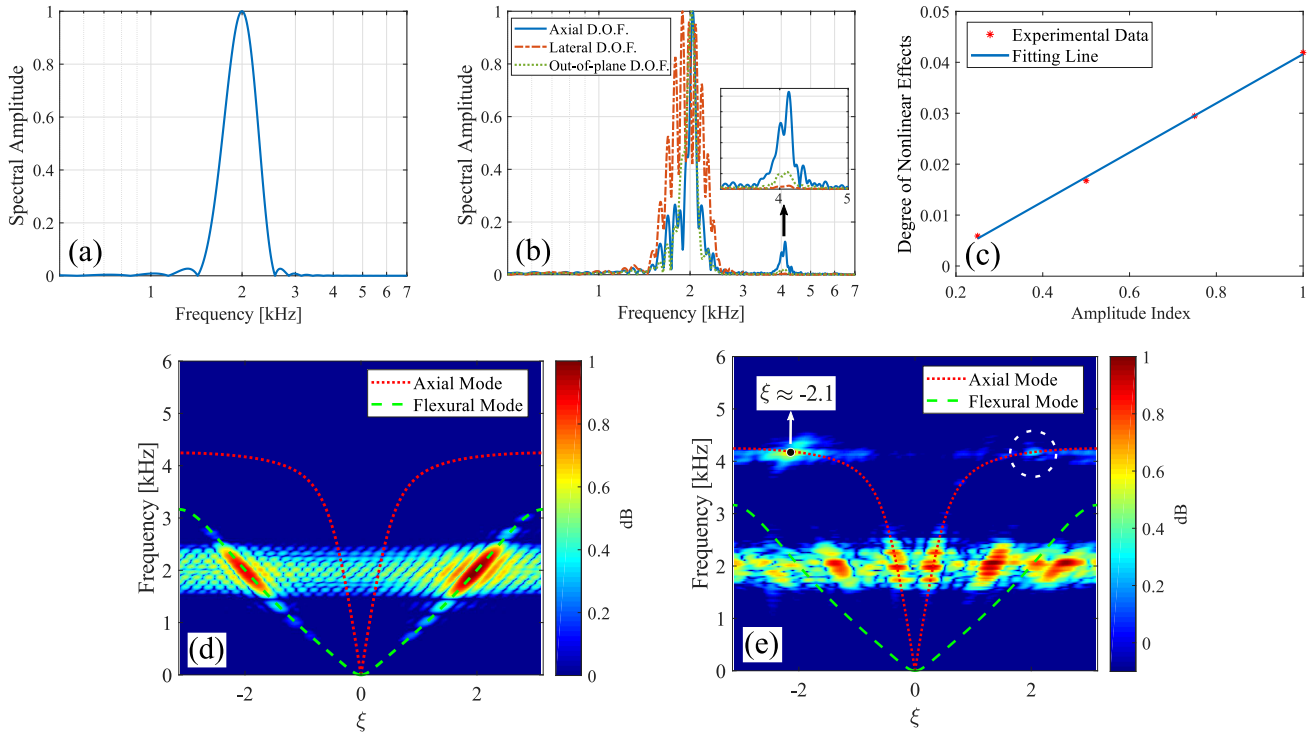

FIG. 4. (a) Frequency spectrum of a tone-burst excitation. (b) Spectral representation of the response collected at a single scan point. (c) Ratio between amplitude of axial second harmonic and amplitude of fundamental flexural harmonic for four different amplitudes (scaled by the maximum value) of excitation. (d) and (e) Spectral representation (via 2D-DFT) of the lateral and axial response, respectively, sampled along the waveguide axis.

modal flexural-to-axial tunneling while enabling phase-matching conditions. To this end, we excite the waveguide laterally with a tone-burst with carrier frequency 2 kHz, whose spectrum is plotted in Fig. 4a. The amplitude of excitation is increased to ensure that sufficient geometrically nonlinear deformations are induced. In Fig. 4b, we plot the frequency spectrum of the total response measured at a representative point located at the mid point of the waveguide (the raw time histories are reported in Supplemental Material [32]). In addition to the dominant contributions at the prescribed excitation frequency, we recognize a strong signature of second harmonic for the axial degree of freedom, while the second harmonic component for the lateral degree of freedom is negligible, in accordance with our previous theoretical findings [21]. In essence, the harmonic generation manifests as a highly mode-selective process in which the axial degrees of freedom dominate the second harmonic despite being a secondary mechanism (only due to coupling) in the fundamental harmonic.

In Fig. 4c we plot the ratio between the amplitude of the axial second harmonic A_{2A} and that of the flexural fundamental harmonic A_{1F} as a function of the amplitude of the fundamental harmonic A_{1F}, for four amplitudes of excitation. The non-constance of this ratio confirms the amplitude-dependent characteristics of the nonlinear response. More specifically, the precise linear trend of the ratio tells us that the intensity of the second harmonic ultimately depends on the square of the amplitude of excitation, consistently with analytical solutions previously obtained for nonlinear waveguides [21]. Through this metric, we can also quantify the strength of the nonlinear effects observed in the response. As a result of the relatively soft modulus of the material and, more importantly, of the activation of phase-matching conditions, the magnitude of the nonlinear features approaches 4% of the amplitude of the fundamental wave, a full order of magnitude stronger than what reported in our previous study [31]. We also note that components of the second harmonic are also observed in the out-of-plane response (green dotted line in Fig. 4b), as further documented in Supplemental Material [32].

Next, we again resort to Fourier analysis to map the dispersive characteristics of the nonlinear response and identify the signature of the second harmonics. The normalized spectral amplitude (in dB units) of the lateral and axial responses is plotted in Fig. 4d and Fig. 4e, respectively. The dispersion curves for the axial and flexural modes are superimposed for reference. In Fig. 4d, the main contribution lies precisely on the flexural branch at the prescribed frequency, while no noticeable flexural features are detected at the second harmonic. In our experiment, the acquisition time is long enough to allow for the fundamental flexural wave to be reflected at

the clamp. This is done to allow the spatial characteristics of the wave to be fully established (Note that we are still in a purely propagating regime, and no standing wave conditions are established). The spatial feature at ω recorded in the left quadrant (negative ξ-space) represents the reflected flexural wave. Due to the damping mechanisms that are present in the structure, the reflected wave is significantly weaker, which can be noticed from the color intensity despite the visual magnification induced by the dB scale. In Fig. 4e, around the excitation frequency, we observe the signature of several modes including: 1) an axial mode induced by the eccentricity in the excitation force; 2) the axial components of the flexural mode, due to bending coupling; 3) two other features associated with out-of-plane modes, also due to coupling as discussed in Supplemental Material [32]. At the second harmonic, we observe one dominant signature located in the negative ξ-space and consisting of two partially overlapping components, one conforming to the folding slope of the axial branch, the other having roughly the same slope of the fundamental flexural branch. These features can be recognized as the homogeneous and forced components of the second harmonic, respectively, which overlap here due to phase-matching conditions. The left quadrant location of these features can be explained invoking notions of aliasing, as graphically illustrated in Fig. 5. Since the wavenumber of the nonlinearly-generated second harmonic ξ_N (here twice the wavenumber of the fundamental wave, centered at 4.1, because of phase-matching conditions) falls outside the irreducible Brillouin zone, it cannot be accurately resolved by the 2D-DFT with our coarse spatial sampling frequency (here $\xi_S = 6.2$, dictated by the one-point per cell limit of our scan). From basic signal processing, the effective wavenumber of the reconstructed second harmonic ξ_R is expected to be

$$\xi_R = \xi_N - \xi_S \approx -2.1 \tag{1}$$

which matches the spectral location of the data. Careful inspection of the right quadrant (positive ξ-space) reveals a second feature at 2ω (highlighted by the dashed white circle in Fig. 4e), albeit significantly smaller in amplitude. We recognize this as the left-going second harmonic due to the reflected component of the fundamental flexural wave. The negligible amplitude here can be attributed to the fact that this is a second-order effect generated by a reflected wave which, as stated above, is already significantly weaker than its incident counterpart due to damping.The right quadrant location of the reflected second harmonic can be explained invoking the same aliasing argument discussed above.

It is important at this point to provide some guarantees that the signatures of nonlinearity observed in the response are predominantly due to the nonlinear mechanics of the problem rather than to other possible sources of nonlinearity, e.g., in the excitation/amplification system,

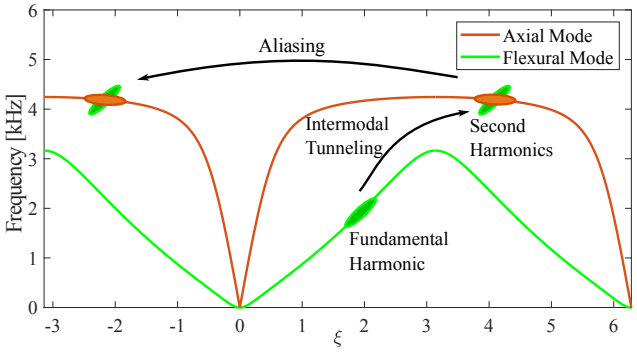

FIG. 5. Schematic illustration of quadrant shift due to aliasing during intermodal tunneling.

or in the contact between the stinger and the structure. The spectral plot of Fig. 4e provides a rationale to support this notion. Consider that, from the perspective of the structure, a nonlinearity in the excitation would essentially be seen as a multi-frequency external input signal, which would therefore trivially activate all the branches of the band diagram that exist at any of the excited frequencies. Accordingly, an externally generated 2ω excitation component would predominantly produce an activation of the 2ω-portion of the axial branch that appears in the right quadrant of the band diagram. This is clearly not the case here where, instead, the positive-ξ axial branch remains essentially de-energized (except the very weak reflected second harmonic discussed above) and the wavenumber of the harmonic is dictated by the peculiar shape of the branches in the band diagram according to the requirements of phase matching conditions. The fact that the harmonic generation is subjected to these modal constraints suggests that the process is indeed controlled by the intrinsic mechanics of the problem. We conclude that, while undoubtedly there is a small nonlinear signature in the external excitation (which is indeed easily detected through an a-priori characterization of the shaker), the bulk of the nonlinear response is to be ascribed to the nonlinearity of the medium.

The multi-resolution capabilities of the 3D SLDV allow us to acquire detailed local snapshots of the wavefield. To this end, a dense grid of scan points spanning over 3 unit cells is used to reconstruct the deflection shapes shown in Fig. 6. The displacement of each point is magnified for visualization purposes and each point is color-coded proportionally to its axial displacement to highlight the activation of the resonators through intermodal tunneling. In Fig. 6a, we plot the fundamental wavefield at four time instants and we recognize the anti-symmetric lateral deflection profile typical of a flexural wave. In Fig. 6b, we use a band-pass filter to distill the contributions at the second harmonic. Displacements and color contrast confirm the activation of strong short-wavelegnth axial mechanisms in the resonators. Compared to Fig. 6a, we

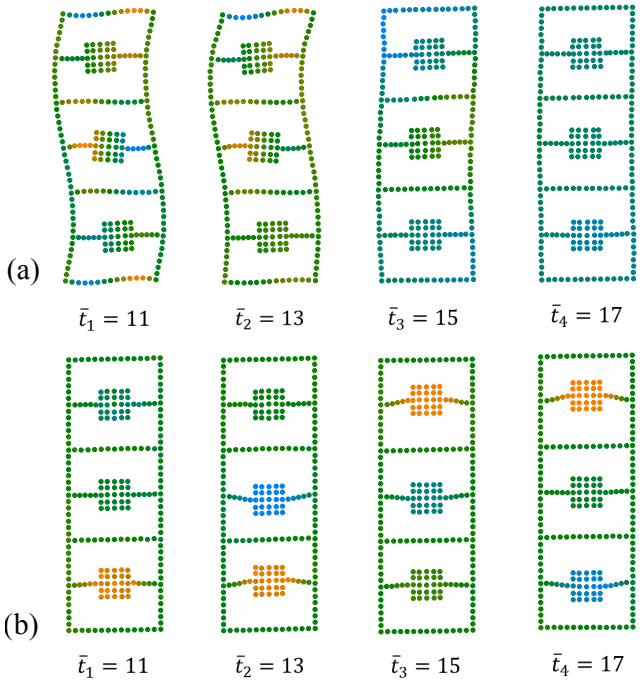

FIG. 6. Experimentally reconstructed internal unit-cell response: snapshots of local wavefield details (spanning 3 cells) at four successive time instants (normalized as $\bar{t}_i = t_i/T$, where $T = 0.5\,\text{ms}$ and $i = 1, 2, 3, 4$). (a) Fundamental flexural wavefield. (b) Filtered wavefield at the second harmonic revealing nonlinear activation of axial resonant mechanisms and energy trapping.

find that the activation of the resonators persists after the flexural packets have traveled through the scanned region, implying that some energy has been transferred to the resonators and locally trapped. If we excited the waveguide axially at the nominal frequency ω, the wavelength would be much larger than the unit cell and therefore bypass the microstructure. To establish comparable effects, it would be necessary to excite at significantly higher frequencies lying on the folding portion of the axial branch. In this respect we can argue that, relatively to purely axial linear phononics, the trapping mechanisms of Fig. 6b display new subwavelength attributes that are directly enabled by intermodal tunneling.

IV. CONCLUSIONS

In summary, we have experimentally studied the propagation of nonlinear waves in a metamaterial waveguide with internal resonators. We have demonstrated the existence of strong intermodal tunneling between flexural and axial mode, thus providing evidence of modal mixing in nonlinear metamaterials. We have acquired detailed scans of the internal unit cell deformation features to visually confirm the modal conversion occurring during tunneling and the strong and persistent energy trapping established in the resonators. We have demonstrated that, by working in nonlinear conditions, strong axial trapping can be achieved even with purely flexural loads and, more importantly, even with low-frequency excitations whose long wavelengths prevent localization in the linear regime. In conclusion, nonlinearity provides an avenue to activate subwavelength phenomena through a simple control of the amplitude of excitation.

ACKNOWLEDGMENTS

The authors acknowledge the support of the National Science Foundation (CAREER Award CMMI-1452488). The authors are grateful to P. Celli and W. Zhang for the many useful discussions and their assistance during the initial stage of the experiments.

[1] Z. Liu, X. Zhang, Y. Mao, Y. Y. Zhu, Z. Yang, C. T. Chan, and P. Sheng, "Locally resonant sonic materials," Science **289**, 1734–1736 (2000).
[2] P. G. Martinsson and A. B. Movchan, "Vibrations of lattice structures and phononic band gaps," Q. J. Mech. Appl. Math. **56**, 45–64 (2003).
[3] P. Celli and S. Gonella, "Low-frequency spatial wave manipulation via phononic crystals with relaxed cell symmetry," J. Appl. Phys. **115**, 103502 (2014).
[4] F. Casadei, T. Delpero, A. Bergamini, P. Ermanni, and M. Ruzzene, "Piezoelectric resonator arrays for tunable acoustic waveguides and metamaterials," J. Appl. Phys. **112**, 064902 (2012).
[5] P. Celli and S. Gonella, "Tunable directivity in metamaterials with reconfigurable cell symmetry," Appl. Phys. Lett. **106**, 091905 (2015).
[6] M. Lapine, I. V. Shadrivov, D. A. Powell, and Y. S. Kivshar, "Magnetoelastic metamaterials," Nature Mater. **11**, 30 – 33 (2012).
[7] Kai Wei, Haosen Chen, Yongmao Pei, and Daining Fang, "Planar lattices with tailorable coefficient of thermal expansion and high stiffness based on dual-material triangle unit," J. Mech. Phys. Solids **86**, 173 – 191 (2016).
[8] P. Celli, S. Gonella, V. Tajeddini, A. Muliana, S. Ahmed, and Z. Ounaies, "Wave control through soft microstructural curling: bandgap shifting, reconfigurable anisotropy and switchable chirality," Smart Mat. Str. **26**, 035001 (2017).
[9] Q. Zhang, K. Zhang, and G. Hu, "Smart three-dimensional lightweight structure triggered from a thin composite sheet via 3d printing technique," Sci. Rep. **6**, 22431 (2016).
[10] K. Bertoldi and M. C. Boyce, "Mechanically triggered transformations of phononic band gaps in periodic elastomeric structures," Phys. Rev. B **77**, 052105 (2008).
[11] B. Florijn, C. Coulais, and Martin van Hecke, "Programmable mechanical metamaterials," Phys. Rev. Lett. **113**, 175503 (2014).
[12] P. Wang, F. Casadei, S. Shan, J. C. Weaver, and K. Bertoldi, "Harnessing buckling to design tunable lo-

cally resonant acoustic metamaterials," Phys. Rev. Lett. **113**, 014301 (2014).

[13] N. Boechler, G. Theocharis, and C. Daraio, "Bifurcation-based acoustic switching and rectification," Nat. Mater. **10**, 665 – 668 (2011).

[14] J.R. Raney, N. Nadkarni, C. Daraio, D.M. Kochmann, J.A. Lewis, and K. Bertoldi, "Stable propagation of mechanical signals in soft media using stored elastic energy," Proc. Natl. Acad. Sci. USA **113**, 9722–9727 (2016).

[15] B. Deng, J. R. Raney, V. Tournat, and K. Bertoldi, "Elastic vector solitons in soft architected materials," Phys. Rev. Lett. **118**, 204102 (2017).

[16] R. K. Narisetti, M. J. Leamy, and M. Ruzzene, "A perturbation approach for predicting wave propagation in one-dimensional nonlinear periodic structures," ASME. J. Vib. Acoust. **132**, 031001 (2010).

[17] Kevin Manktelow, Raj K. Narisetti, Michael J. Leamy, and Massimo Ruzzene, "Finite-element based perturbation analysis of wave propagation in nonlinear periodic structures," Mech. Syst. Signal Process. **39**, 32 – 46 (2013).

[18] M. H. Abedinnasab and M. I. Hussein, "Wave dispersion under finite deformation," Wave Motion **50**, 374 – 388 (2013).

[19] R. Ganesh and S. Gonella, "From modal mixing to tunable functional switches in nonlinear phononic crystals," Phys. Rev. Lett. **114**, 054302 (2015).

[20] R. Ganesh and S. Gonella, "Nonlinear waves in lattice materials: Adaptively augmented directivity and functionality enhancement by modal mixing," J. Mech. Phys. Solids **99**, 272 – 288 (2017).

[21] W.J. Jiao and S. Gonella, "Mechanics of inter-modal tunneling in nonlinear waveguides," J. Mech. Phys. Solids **111**, 1 – 17 (2018).

[22] L. K. Zarembo and V. A. KrasilNikov, "Nonlinear phenomena in the propagation of elastic waves in solids," Sov. Phys. Usp. **13**, 778 (1971).

[23] V. J. Sánchez-Morcillo, I. Pérez-Arjona, V. Romero-García, V. Tournat, and V. E. Gusev, "Second-harmonic generation for dispersive elastic waves in a discrete granular chain," Phys. Rev. E **88**, 043203 (2013).

[24] J. Cabaret, V. Tournat, and P. Béquin, "Amplitude-dependent phononic processes in a diatomic granular chain in the weakly nonlinear regime," Phys. Rev. E **86**, 041305 (2012).

[25] W. J. N. De Lima and M. F. Hamilton, "Finite-amplitude waves in isotropic elastic plates," J. Sound Vib. **265**, 819–839 (2003).

[26] S. P. Wallen and N. Boechler, "Shear to longitudinal mode conversion via second harmonic generation in a two-dimensional microscale granular crystal," Wave Motion **68**, 22–30 (2017).

[27] V. A. Krasilnikov and L. K. Zarembo, "Nonlinear interaction of elastic waves in solids," IEEE Trans. Sonics Ultrason. **14**, 12–17 (1967).

[28] V. Tournat, V. E. Gusev, V. Yu Zaitsev, and B. Castagnede, "Acoustic second-harmonic generation with shear to longitudinal mode conversion in granular media," Europhys. Lett. **66**, 798 (2004).

[29] M. Deng, P. Wang, and X. Lv, "Experimental observation of cumulative second-harmonic generation of lamb-wave propagation in an elastic plate," J. Phys. D: Appl. Phys. **38**, 344 (2005).

[30] K. H. Matlack, J. Y. Kim, L. J. Jacobs, and J. Qu, "Experimental characterization of efficient second harmonic generation of lamb wave modes in a nonlinear elastic isotropic plate," J. Appl. Phys. **109**, 014905 (2011).

[31] R. Ganesh and S. Gonella, "Experimental evidence of directivity-enhancing mechanisms in nonlinear lattices," Appl. Phys. Lett. **110**, 084101 (2017).

[32] See Supplemental Material [URL will be inserted by publisher] for experimental time histories and out-of-plane responses.